Tracking the Immediate and Short-Term Effects of Continuous Theta Burst Stimulation on Dynamic Brain States

Chao Chen, Zhidong Guo, Weiwei Peng, Shengpei Wang, Shuang Qiu, Jing Zhang, Xiaogang Chen, and Huiguang He, *Senior Member, IEEE*

***Abstract*— Continuous Theta Burst Stimulation (cTBS) has been shown to modulate cortical oscillations and induce cortical inhibitory effects. Electroencephalography (EEG) studies have shown some immediate effects of cTBS on brain activity. To investigate both immediate effects and short-term effects of cTBS on dynamic brain changes, cTBS was applied to 22 healthy participants over their left motor cortex. We recorded eyes-open, resting-state EEG and performance in the Nine-Hole Peg Test (NHPT) before cTBS, immediately after cTBS, and 80 minutes after cTBS. We identified nine states using a Hidden Markov Model (HMM)-based approach to describe the process of dynamic brain changes. The spatial activation, temporal profiles of HMM states and behavioral performance of NHPT were assessed and compared. cTBS altered the temporal profiles of S1-S5 immediately after cTBS and the temporal profiles of S5, S6 and S7 80 min after cTBS. Moreover, cTBS improved motor function of the left hand. State 1 was characterized as the activation of right occipito-temporal area, and NHPT behavioral performance of the left hand positively correlated with the occurrence of state 1, and negatively correlated with the interval time of state 1 after cTBS. The transitions between S1 or S7 and other states showed dynamic reconfiguration during after-effect sustained time after cTBS. These results suggest that the dynamic characteristics of state 1 are potential biomarkers for characterizing the aftereffect changes of cTBS.**

***Index Terms*— Continuous theta burst stimulation, resting-state EEG, hidden Markov model, brain state.**

Manuscript received 8 October 2023; revised 18 February 2024; accepted 14 March 2024. Date of publication 25 March 2024; date of current version 29 March 2024. This work was supported in part by the National Key Research and Development Program of China under Grant 2022YFC3602803, in part by the National Natural Science Foundation of China under Grant 62276262 and Grant 62201569, in part by the Natural Science Foundation of Guangdong Province under Grant 2022A1515011097, and in part by the Beijing Natural Science Foundation under Grant 7222311 and Grant J210010. *(Corresponding authors: Shengpei Wang; Shuang Qiu; Huiguang He.)*

Chao Chen and Zhidong Guo are with the Key Laboratory of Complex System Control Theory and Application, Tianjin University of Technology, Tianjin 300387, China.

Weiwei Peng is with the School of Psychology, Shenzhen University, Shenzhen 518060, China.

Shengpei Wang and Shuang Qiu are with the Laboratory of Brain Atlas and Brain-Inspired Intelligence, Key Laboratory of Brain Cognition and Brain-inspired Intelligence Technology, and the School of Artificial Intelligence, University of Chinese Academy of Sciences, Institute of Automation, Chinese Academy of Science, Beijing 100045, China (e-mail: wangshengpei2014@ia.ac.cn; shuang.qiu@ia.ac.cn).

Jing Zhang is with the Neurology Department, Beijing Tiantan Hospital, Capital Medical University, Beijing 100070, China.

Xiaogang Chen is with the Institute of Biomedical Engineering, Chinese Academy of Medical Sciences and Peking Union Medical College, Tianjin 300192, China.

Huiguang He is with the Laboratory of Brain Atlas and Brain-Inspired Intelligence, the Key Laboratory of Brain Cognition and Brain-inspired Intelligence Technology, the Institute of Automation, Chinese Academy of Science, and the School of Artificial Intelligence, University of Chinese Academy of Sciences, Beijing 100045, China (e-mail: huiguang.he@ia.ac.cn).

Digital Object Identifier 10.1109/TNSRE.2024.3378712

I. Introduction

REPETITIVE transcranial magnetic stimulation (rTMS) is a non-invasive brain stimulation method that involves delivering repeated stimulation pulses through a magnetic field to modulate cortical activity in specific brain regions, thereby influencing cortical excitability [1], [2], [3]. rTMS is widely used to promote functional recovery after stroke. Previous studies have demonstrated that the application of high-frequency rTMS to the affected hemisphere and low-frequency rTMS to the unaffected hemisphere in stroke patients yields promising results in motor function recovery [4], [5].

Theta burst stimulation (TBS) is a promising rTMS protocol that has similarities in stimulation effects with conventional rTMS [6], [7]. However, TBS has a longer aftereffect duration time and a shorter application time and is receiving increasing attention in neuroscience research and clinical treatment [8], [9]. The continuous TBS (cTBS) protocol has been shown to induce inhibitory effects, which is similar to low-frequency rTMS [8], [9], [10], [11]. cTBS is increasingly being applied in motor function recovery after stroke [12], [13]. However, the mechanisms of cTBS are still unclear. Therefore, some research has been conducted to explore the mechanisms and lasting effects of TBS on brain cortical plasticity, as well as its role in improving motor function [14], [15].

In the early stages of rTMS research, motor evoked potentials (MEPs) were widely used to study cortical plasticity [16], [17]. MEP mainly depends on the excitability of spinal motor neurons and does not directly reflect cortical plasticity mechanisms [18]. Since rTMS directly stimulates the brain, it triggers changes in brain activity, leading to behavioral changes. Combining rTMS with other neuroimaging methods can also provide a more comprehensive understanding of its effects and potential mechanisms [19]. Two widely used

neuroimaging methods for measuring cortical responses to TMS are functional magnetic resonance imaging (fMRI) and electroencephalography (EEG). Compared to fMRI, EEG is often used to capture rapid changes in brain activity over time due to its high temporal resolution. In addition, EEG offers ease of operation and is suitable for long-term monitoring, making it widely used for application in rTMS research. EEG enables researchers to quantify and characterize activation patterns in the temporal and spatial domains [20], [21]. Therefore, this study provides valuable insights into the effects of rTMS on brain activity and functional changes.

Resting-state EEG (rsEEG) is considered a valuable reflection of the brain's intrinsic spontaneous activity and is closely linked to its functional connectivity and regulation [22], [23], [24]. Many studies have analyzed and compared rsEEG before and after rTMS to gain insights into the effects of rTMS on brain activity. This approach not only circumvents the indirect impact of MEPs on cortical spinal excitability and rTMS-evoked potential electromagnetic interference but also provides a more precise avenue for investigating the brain's response to rTMS stimulation [25]. In 2021, Zhong et al. applied 10 Hz rTMS in patients with unilateral brain lesions and found a decreased power of delta oscillations in the ipsilesional hemisphere immediately after rTMS, whereas distinct cortical oscillations were observed in the alpha band around the parietal-occipital lobe in the contralesional hemisphere [26]. In 2022, Ding et al. explored the effects of intermittent TBS (iTBS) on the functional network of rsEEG and found a significant increase in interhemispheric functional connectivity in the delta and theta frequency bands immediately after stimulation [27]. In 2023, Jin et al. found that high-frequency rTMS with a 2 s train duration and 25 s intertrain interval increased cortex excitability and the power spectral density of bilateral central regions in the alpha frequency band and enhanced the functional connectivity between central regions and other brain regions [28]. These studies collected EEG signals within 30 minutes after rTMS and analyzed the aftereffects within 30 minutes after rTMS.

Research on MEPs has demonstrated that the effects of rTMS can persist for up to 90 minutes after stimulation [29]. Several studies have analyzed the changes in brain activity in different periods after stimulation. Stren et al. recorded rsEEG before, immediately after, 25 minutes after, and 50 minutes after 1 Hz rTMS. rTMS caused a significant increase in ipsilateral EEG coherence and in the interhemispheric coherence between motor areas in the alpha band. This effect lasted up to 25min post-stimulation [30]. In our previous study, we found that within the alpha band, functional connectivity decreased immediately after rTMS, but it significantly increased 20 minutes after rTMS [31]. Qiu et al. recorded rsEEG and behavioral performance before and in multiple sessions up to 90 min after cTBS. Although this work did not report a significant change in the microstate matrixes of rsEEG, it indicated that cTBS over the motor cortex induced a modulation effect specific to microstate B dynamics [32]. These few studies have utilized neural oscillation analysis, network analysis and microstate analysis to explore rsEEG changes at different time points after rTMS/cTBS. Although they found some immediate changes after rTMS/cTBS through analyzing rsEEG after rTMS, they did not report significant short-term changes based on these rsEEG analyses. It may be due to the inability of the methods already in use to effectively capture these changes. Therefore, it is necessary to apply novel analyses to investigate short-term effects after stimulation, which is helpful in achieving a deep understanding of the effects of stimulation on brain activity.

The Hidden Markov Model (HMM) characterizes brain activity as a dynamic sequence of discrete brain states, each with distinct network activity features. Hunyadi et al. simultaneously recorded EEG and fMRI data in conjunction with HMM [33]. They discovered that the fMRI correlates of fast transient EEG dynamic networks exhibit highly reproducible spatial patterns. Moreover, the spatial organization of these patterns demonstrates a strong resemblance to traditional fMRI resting-state network maps. Both the microstate analysis and the HMM analysis can lead to state lifetimes on the 100 ms timescale. Coquelet et al. compared the microstate method with the HMM method, and they suggested that the Kmeans-based microstate analysis mainly focuses on topological clustering at local maximum global field power (GFP) time points, particularly emphasizing high-power activity. In contrast, the power envelope analysis based on HMM has its uniqueness, encoding states based on spatial patterns of oscillatory power over continuous time, enabling finer detection of temporal-scale states [34]. Therefore, the HMM method focuses on transitions between low and high power in the power envelope and is more sensitive to these transitions, thus potentially capturing power activity more finely. Moreover, in terms of state detection, the Kmeans-based microstate method tends to focus on four standardized microstate maps, and related research has clearly defined these four microstates. The HMM method usually identifies more states, which suggests HMM's high flexibility and sensitivity in capturing dynamic changes in brain states. Most importantly, HMM is not limited to identifying features at specific time points; it reflects the activation characteristics of brain networks [34]. In addition, HMM demonstrates excellent temporal characteristics, effectively tracking and analyzing the dynamic changes in brain activity over time. This is extremely important for gaining a deeper understanding of brain function and processing mechanisms. Compared with the microstate method used in our previous study [32], the HMM method has the potential to explore both immediate effect and short-term effect. Therefore, in this study, we aimed to adopt the HMM method to investigate the immediate effect and short-term effect induced by cTBS.

This study aims to investigate the immediate and short-term changes in behavior and brain dynamics induced by cTBS and characterize the relationship between brain state based on HMM and behavior performance after cTBS. We applied cTBS to the left primary motor cortex (M1) region and recorded open-eyes rsEEG data and tested the Nine-Hole Peg Test (NHPT) of each hand before stimulation (Pre), immediately after stimulation (I-Post), and 80 minutes after stimulation (S-Post). Here, the NHPT was applied to measure hand dexterity. We described the temporal characteristics of

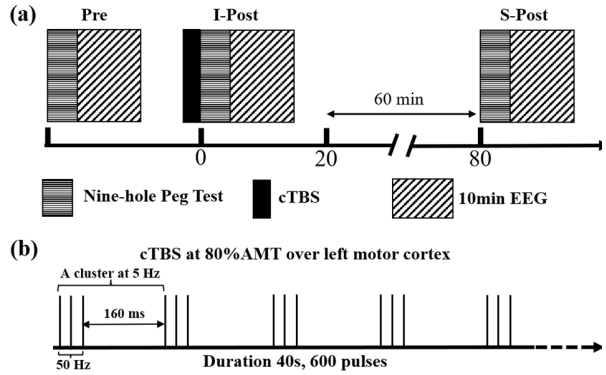

Fig. 1. Experimental Paradigm. (a) Overview of the experimental process, including three sets of behavioral measurements and EEG data recorded before cTBS (Pre), immediately post-cTBS (I-Post), and 80 minutes after cTBS (S-Post). (b) rTMS stimulation protocol illustrating the application of a 40-second (600 pulses) cTBS paradigm, repeating three bursts of 50 Hz pulses with a 200-millisecond interval.

HMM states and their corresponding activation networks at different sessions. Additionally, we assessed the relationship between HMM state features and behavioral task completion times using correlation analysis.

II. Methods

A. Participants

Twenty-two right-handed healthy subjects (12 males and 10 females, average age 22.3 ± 2.0 years (mean ± standard deviation) ranging from 18 to 25 years) were recruited in institute of Automation, Chinese Academy of Sciences, Beijing, China. All subjects met the following inclusion criteria: (1) not taking any psychotropic medication; (2) no prior history of neurological or psychiatric disorders; (3) no family history of such conditions; and (4) passing the safety screening for rTMS. In addition, this study was approved by the Institutional Review Board of the Chinese Academy of Science. All subjects signed an informed consent form.

B. Experimental Paradigm

This study utilized data from the dataset in our previous study [32]. The details of the experiment have been reported in the previous study, thus we briefly introduce the experiment here. The experimental procedure is visualized in Figure 1(a). Prior to cTBS stimulation (Pre), each participant completed a set of behavioral tasks with each hand, followed by a 10-minute recording of rsEEG. After an appropriate rest period, participants received a single session of cTBS lasting 40 seconds. Subsequently, behavioral tasks and rsEEG were recorded for each hand immediately after cTBS (I-Post) and again 80 minutes post-cTBS (S-Post).

We utilized the Nine-Hole Peg Test (NHPT) as the behavioral task, employing a Nine-Hole Pegboard Kit (Jamar, Chicago, USA) for testing. The completion time, measured in seconds, served as the performance metric, and participants were instructed to perform the task sequentially with their left hand followed by their right hand. Prior to the start of the experiment, participants received instructions and practice for the NHPT task to ensure their familiarity and efficient performance. During rsEEG data collection, participants were instructed to keep their eyes open, minimize body and head movements, and avoid systematic thinking, all of which helped to ensure the accuracy of brain activity recording.

In this experiment, we employed the cTBS paradigm, as shown in Figure 1(b). This paradigm involved continuous stimulation for 40 seconds (total of 600 pulses), with triplets of 50 Hz stimulation pulses repeated every 200 ms. The cTBS stimulation was delivered using an M-series stimulator manufactured by YINGCHI (Shenzhen, China). During the stimulation process, we positioned the coil specifically in the left primary motor cortex (M1) region, ensuring that it remained tangent to the scalp. This positioning was based on identifying the optimal coil position for inducing a motor response in the first dorsal interosseous muscle (FDI) of the contralateral thumb. To determine the appropriate stimulus intensity for cTBS, we set it at 80% of the active motor threshold (AMT). The AMT was defined as the lowest stimulus intensity that elicited a motor response. During 10 consecutive stimulation trials of static contraction of the right FDI muscle, at least 5 stimuli were required to elicit a motor response of 200 microvolts, with the participant maintaining a maximal autonomic contraction of approximately 20%. This ensured consistent and reliable motor responses during the experiment.

C. EEG Data Acquisition and Preprocessing

We employed a 64-channel BrainAmp MRplus system (BrainProducts Inc., Munich, Germany) to acquire EEG data following the international 10–20 system. During the acquisition, FCz and AFz were used as the ground and reference electrodes, respectively. Additionally, a separate channel was used to record the electrocardiogram signal, resulting in a reduction in the number of EEG electrodes to 63. To ensure high-quality acquisition, electrode impedances were maintained below 10 kΩ. The sampling rate was set at 5,000 Hz, and a frequency filter was applied in-line to cover the range from DC to 200 Hz, with additional notch filtering carried out at 50 Hz to eliminate line noise interference. These measures were taken to ensure reliable and accurate EEG data collection during the experiment.

We performed offline processing of the EEG data using the EEGLAB v2022.1 toolbox within the MATLAB R2021a environment. For each continuous 10-minute rsEEG session, the preprocessing steps for the data are shown in Figure 2(a). Initially, the rsEEG data were bandpass filtered within the frequency range of 0.5 to 30 Hz. Subsequently, to facilitate further analysis, the sampling frequency was downsampled to 250 Hz. Furthermore, automatic detection of bad channels was executed employing available tools in EEGLAB, and any identified bad channels were subsequently interpolated using information from neighboring channels. Independent component analysis (ICA) processing was then conducted utilizing the MARA toolbox in EEGLAB to effectively eliminate artifacts related to eye, heart, and muscle activities, thereby enhancing the overall data quality. Following the completion of these aforementioned steps, we removed the

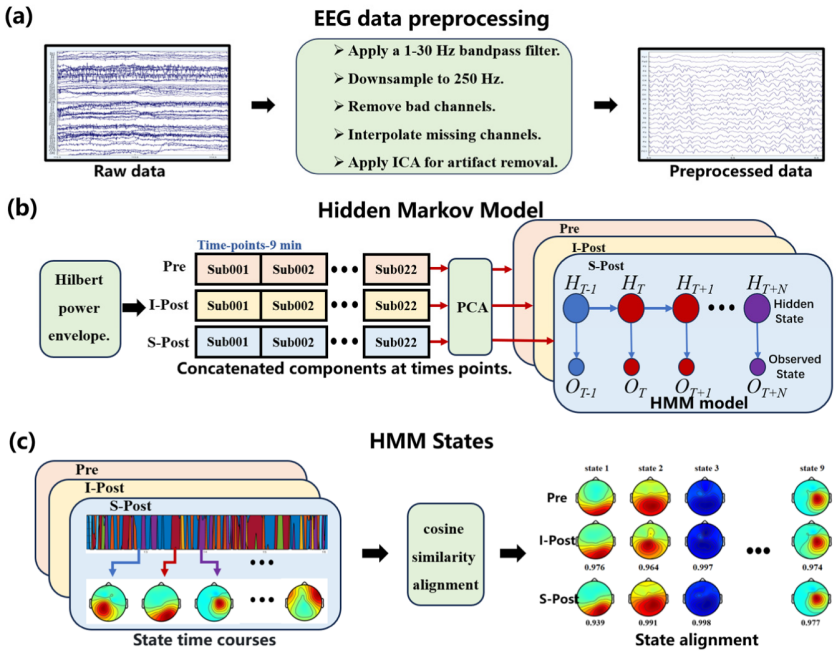

Fig. 2. (a) The preprocessing of the electroencephalogram (EEG) data involves multiple steps. (b) shows the process before model inference, involving calculating EEG data's Hilbert power envelope, data concatenation, Principal Component Analysis (PCA), and inputting into the HMM for inference. (c) The inference results of the HMM are aligned using cosine similarity.

initial 30 seconds and the final 30 s of each rsEEG segment to facilitate subsequent EEG data analysis.

D. Hidden Markov Model

The Hidden Markov Model (HMM) is a probabilistic model for time sequences that describes a time series as a sequence of states, each with its own observation data model. The HMM approach avoids the limitations of traditional microstate modeling methods and is currently widely applied in MEG and fMRI research. Therefore, we identified brain states from the EEG of three sessions through the HMM approach. As shown in Figure 2(b), we further processed each electrode channel of rsEEG segments, including removing the linear trend and applying the Hilbert transform to retain only the amplitude information, which was then normalized to obtain rsEEG amplitude envelopes. Subsequently, we concatenated the amplitude envelopes of all participants within the same session along the temporal dimension, thus creating three group-level amplitude envelope matrices Y, with dimensions being $N_{channel} \times (N_{subject} \times N_{timepoint})$, where $N_{channel} = 63$, $N_{subject} = 22$, and $N_{timepoint} = 135000$ (Sampling rate: 250Hz, the duration of data: 9 minutes). We performed a cross-channel Principal Component Analysis (PCA) on these three groups of amplitude envelopes, aiming to achieve dimensionality reduction, thereby reducing the computational burden. It's noteworthy that too high explained variance can lead to model overfitting, while too low explained variance might result in loss of information, affecting the interpretability of the model. The dimension of the reduced data matrix $Y_{reduced}$ becomes $N_{PC} \times (N_{subject} \times N_{timepoint})$. Our choice was based on the results of multiple comparisons, ultimately deciding to retain approximately 21 principal components (explaining 90% of the variance). Next, we modeled the power envelope of resting-state brain activity using the HMM-Gaussian model. The HMM-Gaussian model assumed that the observed data (i.e., EEG time series) are generated from these brain states through a multivariate Gaussian distribution, including the covariance matrix and the mean distribution.

It is noteworthy that a major challenge in applying HMM lies in the need to pre-determine the number of states in the model (i.e., the K value). Traditionally, the selection of the number of states in HMMs is based on the principle of minimizing free energy, but we have observed that free energy tends to decrease monotonically as the number of states increases. Therefore, following the research methods of Baker et al. [46], we utilized statistical metrics of state occupancy to determine the optimal number of states. In our analysis of HMMs with state numbers ranging from 4 to 20, we calculated the maximum, minimum, and median values of state occupancy for each state number. We found that at 9 states, there is a significant inflection point in the minimum value of state occupancy. Additionally, with the number of states set at 9, we repeatedly ran the model to assess the robustness of state identification. The results show that state identification maintained a high level of consistency across multiple runs when the number of states was 9. Therefore, in this study, we chose to set the number of states at 9.

E. State Alignment

We back-projected the state-specific mean distributions to the EEG channel space using the inverse of the mixing matrix (M^T) from PCA decomposition, creating averaged activation maps for each HMM-based state. Cosine similarity, as a matching measure, can effectively quantify the similarity

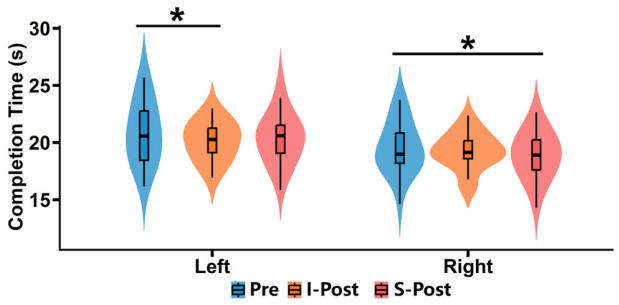

Fig. 3. Distribution and significance test results for left-hand and right-hand NHPT completion times ('*' represents $p < 0.05$).

in the locations of high-power activities across different states [33], [34]. Upon successfully estimating the group-level data for Pre, I-Post, and S-Post, we conducted a comparative analysis using cosine similarity (Figure 2(c)). Utilizing the estimation results from Pre as the reference, we assessed their similarity against the estimation results from I-Post and S-Post. Cosine similarity values span from -1 to 1, with higher values signifying greater resemblance between activated regions. Subsequently, we computed the similarity between all states in Pre and all states in I-Post and S-Post, selecting the maximum value as the matching result. Through matching, we ensured the comparability of data at different time points, enabling a more accurate comparison of differences between states at different time points and further analysis of the effects of stimulation on neural activity.

F. HMM Global Statistics

The HMM inference results present us with invaluable state time courses, offering insights into the dynamic behavior of the brain during different cognitive states. These time courses elucidate the probability of each state being active at each time point, offering a detailed representation of the brain's activity patterns across various experimental conditions. Through the use of the Viterbi algorithm, we can accurately map each time point to its corresponding state, resulting in a clear and comprehensive state time course matrix. The state time course matrix plays a crucial role in uncovering the temporal properties of each brain state. This matrix enables us to quantify and analyze the dynamic characteristics of brain activity for each subject per session using a set of carefully computed temporal metrics, including (1) state fractional occupancy, which refers to the percentage of total time that each state occupies in the entire EEG recording. (2) State occurrence refers to the average number of times each state appears per second. (3) The state interval time refers to the average time interval between two consecutive occurrences of the same state.

Furthermore, this method allows for the explicit estimation of state transition probabilities, thereby providing a more accurate description of the dynamic evolution of brain networks. State transition probability refers to the probability of transitioning from one state to another within the sequence of states.

G. Statistical Analysis

In this study, we employed a one-way repeated measures Analysis of Variance (ANOVA) to assess the effect of session on the completion time of behavioral task and the temporal indicators of each state (state occupancy, occurrence rate, and interval time). Before conducting statistical analyses, we evaluated the normality of the data using the Shapiro-Wilk test. Also, we applied the Mauchly's test of sphericity to ensure the assumption of sphericity. Repeated measures ANOVA was performed in: (1) Section III-A Behavioral results (Figure 3); (2) Section III-A. State Temporal Characteristics (Figure 5); (3) Section III-E. State Transition (Figure 7). Paired t-tests were conducted to assess differences between paired data. A significance level was set at 0.05. All statistical results reported in this paper have been Bonferroni corrected, and adjusted p-values are reported. T-tests in (1) Section III-A Behavioral results (Figure 3) compared NHPT completion times between each of the three sessions, resulting in two comparisons; (2) Section III-A. State Temporal Characteristics (Figure 5) also involved t-tests, comparing each state' temporal characteristics between each of the three sessions, resulting in two comparisons; (3) Section III-E. State Transition (Figure 7) involved t-tests comparing everyone's state transitions in the Pre session with those in the I-Post and S-Post sessions, leading to two comparisons. Finally, in Section III-D of this article, we used Pearson correlation analysis to calculate the correlations between each measure and the completion time of NHPT, to evaluate the strength and statistical significance of these correlations with NHPT completion times. All statistical analyses were performed using SPSS software (IBM SPSS Statistics, IBM Corporation).

III. Result

A. Behavioral Results

Figure 3 depicts the completion times of the NHPT at each session for each hand. A one-way repeated-measures ANOVA revealed that there was a significant effect of cTBS on completion times of NHPT for either the left hand ($F(2, 42) = 3.092$, $p < 0.05$) and the right hand ($F(2, 42) = 3.657$, $p < 0.05$) NHPT. Post hoc analysis revealed that the completion time of NHPT for the left hand during the I-Post session was significantly shorter than that during the Pre session ($p < 0.05$). The time of NHPT during the S-Post session tended to be shorter after cTBS ($p = 0.16$). This indicates significant motor function improvement of the left hand immediately after cTBS over the left motor cortex. For the right hand, the completion time in the S-Post session was significantly shorter than that in the Pre session ($p < 0.05$). This may be due to the practice effect of NHPT.

B. State Spatial Feature

Figure 4 illustrates the average activation maps for each state extracted in the three sessions. Therefore, cosine similarity was calculated to align the three sessions of states, using the maps in the Pre session as the baseline. We labeled these

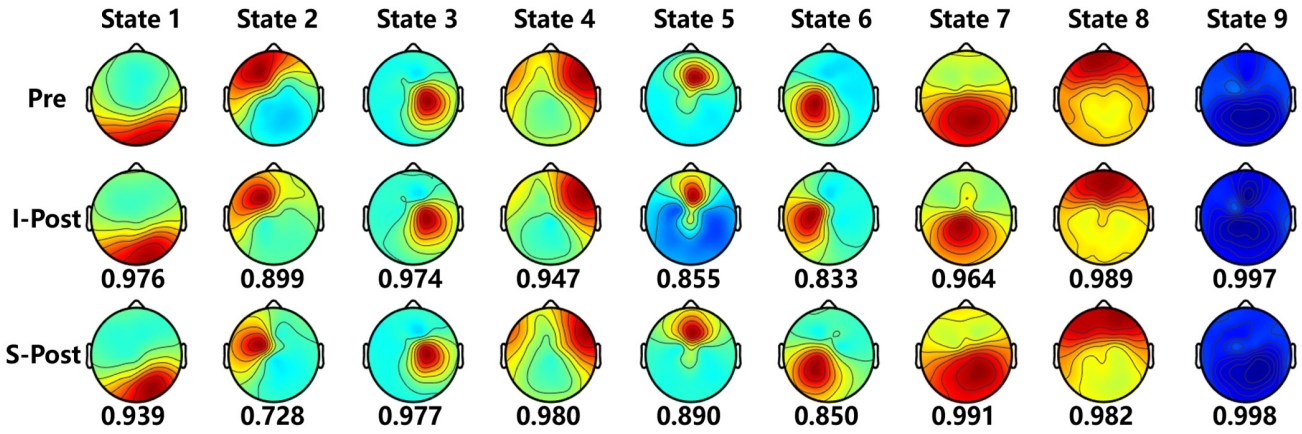

Fig. 4. State alignment results. The cosine similarity of each state in the I-Post and S-Post sessions relative to the corresponding state in the Pre session is provided below each state in the figure.

states as State 1 to State 9 and named them S1 to S9, respectively. These maps locate significant power increases/decreases upon HMM state activation. S1 involved activation in the right occipital- temporal junction. S2 displayed a pattern of activation in the frontal cortex in the left hemisphere, while S4 displayed a pattern of activation in the frontal cortex in the right hemisphere. S3 and S6 displayed a pattern of activation in the left and right hemispheric central regions, respectively. S5 involves activation in the frontoparietal region. S7 involved parietal activation along with prefrontal deactivation, and S8 showed an opposite pattern of prefrontal activation and parietal activation. These two states are thus reminiscent of a dynamical top-down attentional control between the prefrontal and parietal regions. S9 corresponds to a state with global modulation of neural activity. Moreover, we used the states in the I-Post and those in S-Post sessions as the baseline separately, and then aligned the other two sets of states with this baseline. We found that alignment results are consistent using each session as the baseline in this study.

The results revealed that states S1, S3, S4, S7, S8 and S9 exhibited relatively high average similarity across the three sessions, whereas states S2, S5, and S6 showed slightly low average similarity. Therefore, cTBS induced a change in the spatial pattern of S2, S5 and S6.

C. State Temporal Characteristics

In all sessions, the average duration of HMM states ranged from approximately 30 to 160 ms, which is consistent with previous research findings [33], [36], [37].

Figure 5 displays the results of crucial characteristics (state fractional occupancy, state occurrence, and state interval time) for the nine states in three sessions. As shown in Figure 5(a), one-way repeated-measures ANOVAs show a significant main effect of session on state fractional occupancy for each state except S8 (all except S8: $p<0.05$; S8: $p=0.7$). Post hoc comparisons revealed that fractional occupancy for S2, S3 and S6 significantly decreased immediately after cTBS, whereas the reverse was true for S4 and S5 ($p<0.05$). In the S-post, fractional occupancy for S4 and S5 was significantly higher than that in the Pre, whereas the reverse was true for S7 ($p<0.05$).

As shown in Figure 5(b), one-way repeated-measures ANOVAs show a significant main effect of session on state occurrence for each state except S8 (all except S8: $p<0.05$; S8: $p=0.17$). Post hoc comparisons revealed that the frequency for S1, S2 and S3 significantly decreased immediately after cTBS, whereas S4 and S5 were more frequent immediately after cTBS ($p<0.05$). In S-Post, the frequency for S5 was significantly higher than that in Pre, whereas the reverse was true for S6 and S7 ($p<0.05$).

As shown in Figure 5(c), one-way repeated-measures ANOVAs show a significant main effect of session on state interval time for each state except S3 and S8 (all except S3 and S8: $p<0.05$; S8: $p=0.056$ S8: $p=0.17$). Post hoc comparisons showed that the interval time for S1, S2 and S9 increased immediately after cTBS, whereas that for S4 and S5 decreased ($p<0.05$). The interval between S6 and S7 was longer in the S-Post group than in the Pre.

These results suggest that cTBS altered the temporal profiles of S1-S5 immediately after cTBS and the temporal profiles of S5, S6 and S7 80 min after cTBS. S1, S2, and S3 occurred less often with longer intervals immediately after cTBS. S4 and S5 occurred more often with short intervals immediately after cTBS, leading to an increase in the percentage of total time that S4 and S5 occupied in the entire EEG recording. 80 min after cTBS, the increase in the percentage of the total time of S4 and S5 remained. 80 minutes after cTBS, S6 and S7 occurred less often, and the interval time was long.

D. Relationship Between HMM States and Behavioral Performance

For the performance of the behavioral task, two significant differences were found (Figure 3), which included one immediate effect on the left hand and one short-term effect on the right hand. Correlation analyses between each of these two differences and each of the brain state indices (state fractional occupancy, state occurrence, and state interval time) with significant differences were performed across the participants.

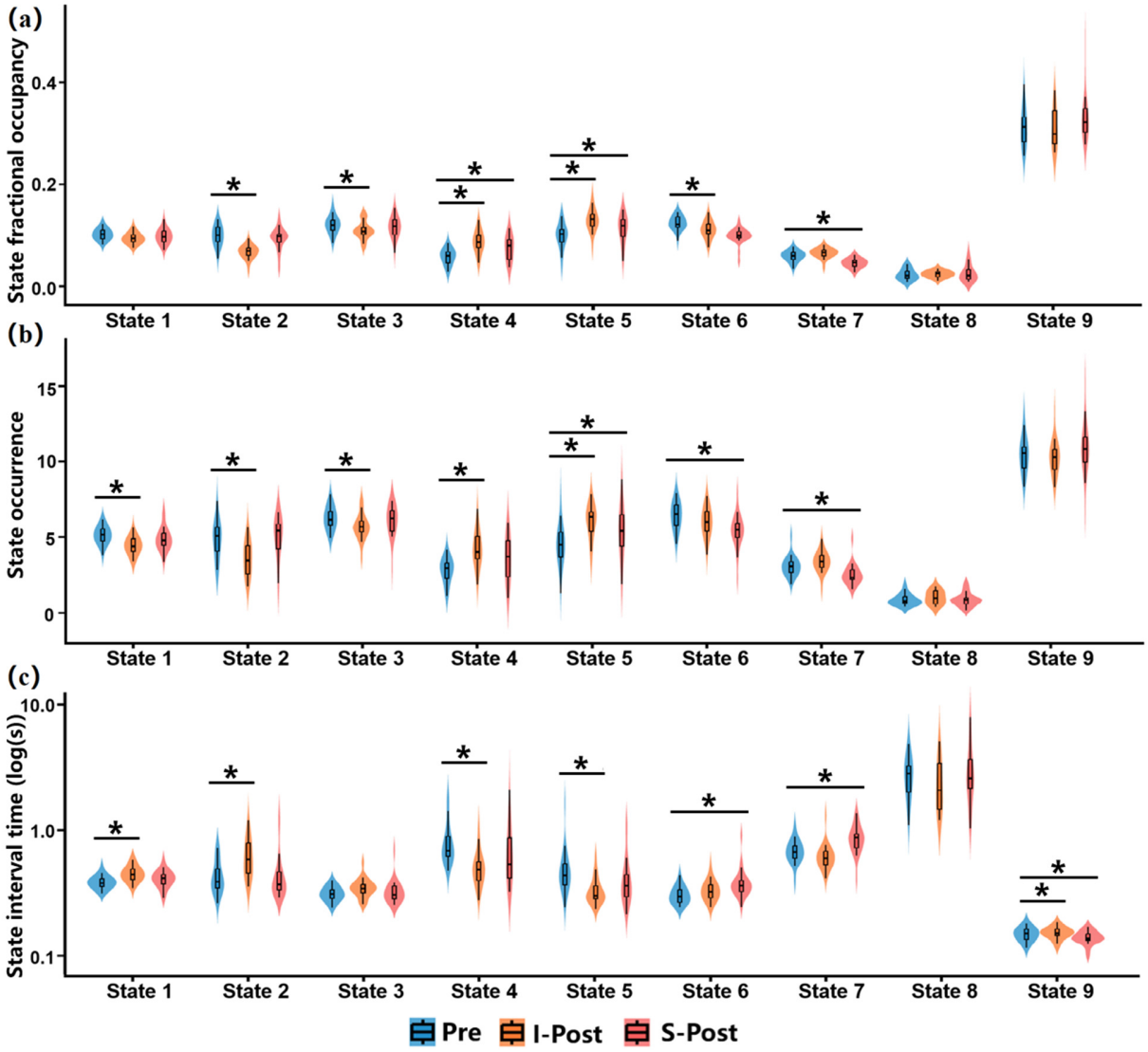

Fig. 5. Distribution of time characteristics state fractional occupancy (a), state occurrence (b), state interval time (c) for each state and results of significance statistical tests ('*' represents $p < 0.001$).

As shown in Figure 6(a), based on the sessions between Pre and I-Post, the occurrence of S1 was found to be significantly positively correlated with the completion time of the left hand NHPT (Pearson's rho = 0.387, $p < 0.01$). This corresponds to the immediate effect where, as shown in Figure 5(b), there was a reduction in the occurrence of S1, and as depicted in Figure 3, there was a decrease in the completion time for the left hand NHPT. Moreover, the interval time of S1 was significantly negatively correlated with the completion time of the left hand NHPT (Pearson's rho = −0.361, $p<0.05$), corresponding to the immediate effect where, as shown in Figure 5(c), the interval time of S1 increased and, as shown in Figure 3, the completion time for the left hand NHPT decreased. As illustrated in Figure 6(b), according to the sessions between Pre and S-Post, the occurrence of S7 was significantly positively correlated with the completion time of the left hand NHPT (Pearson's rho = 0.363, $p<0.05$). This is in line with the short-term effect, where as depicted in Figure 5(b), there was a reduction in the occurrence of S7, and as shown in Figure 3, there was a decrease in the completion time for the right hand NHPT. Furthermore, the interval time of S7 was significantly negatively correlated with the completion time of the left hand NHPT (Pearson's rho = −0.333, $p<0.05$), which aligns with the short-term effect, where as shown in Figure 5(c), the interval time of S7 increased and, as depicted in Figure 3, the completion time for the right hand NHPT decreased.

These results indicate that immediately after cTBS, individuals with better NHPT performance for the left hand showed a higher state occurrence of S1 and a lower state interval time of S1. Additionally, 80 minutes after cTBS, individuals with better NHPT performance for the right hand showed a higher state occurrence of S7 and a lower state interval time of S7. This suggests that the modulation of S1 and S7 induced by cTBS influences motor function.

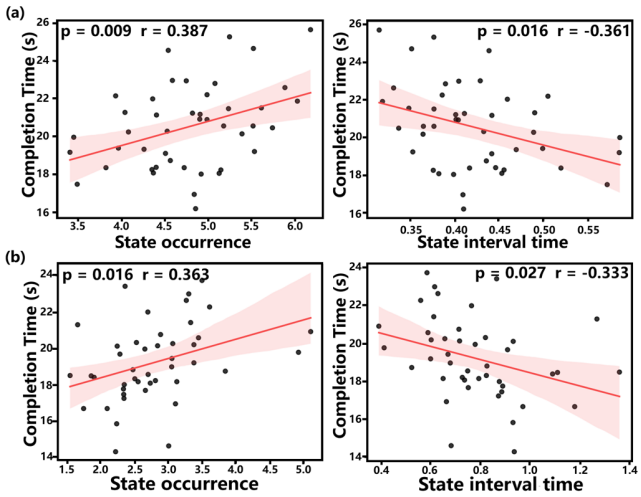

Fig. 6. The Pearson correlation between NHPT completion time and brain states is shown. Pearson correlation values (r) and p values are provided. The red shaded area represents a 95% confidence interval. (a) represents the correlation between the immediate-term (Pre and I-Post) left-hand NHPT completion time and the state occurrence and state interval time of state S1. (b) represents the correlation between the short-term (Pre and S-Post) right-hand NHPT completion time and the state occurrence and state interval time of state S7.

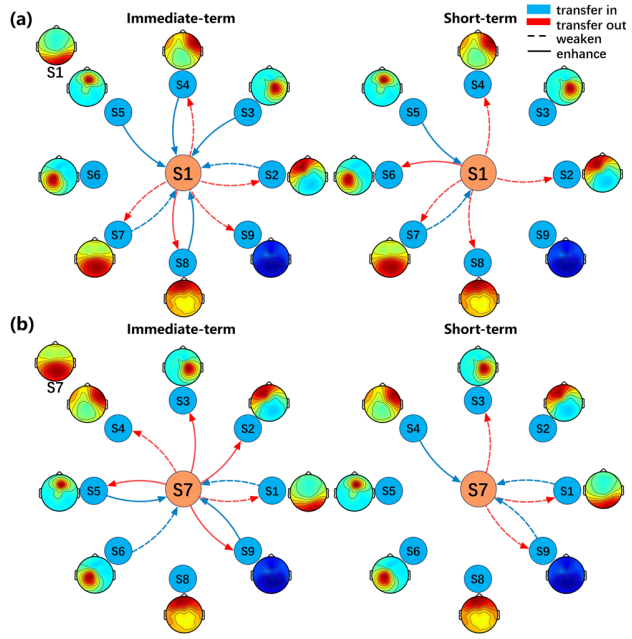

Fig. 7. Changes in the transition probabilities of states S1 and S7. (a) represents the state transition changes of state S1 between the immediate -term and short-term sessions. (b) represents the state transition changes of state S7 between the immediate-term and short-term sessions.

E. State Transitions

Considering that the correlation between brain state indices and NHPT completion times is primarily concentrated in S1 and S7, the state transition changes of these two states during the immediate-term (Pre vs. I-Post) and short-term (Pre vs. S-Post) intervals are displayed in Figure 7.

Figure 7(a) shows the changes in state transitions for S1. During the immediate-term interval, the transition probabilities from S1 to S2, S4, S7, and S9 significantly decreased ($p < 0.05$), while the transition probability from S1 to S8 increased ($p < 0.05$). The transition probabilities from S2 and S7 to S1 decreased ($p < 0.05$), while the transition probabilities from S3, S4, S5, and S8 to S1 increased ($p < 0.05$). During the short-term interval, the transition probabilities from S1 to S2, S4, S7, and S8 decreased ($p < 0.05$), while the transition probability from S1 to S6 increased ($p < 0.05$). The transition probability from S5 to S1 increased ($p < 0.05$), while the transition probability from S7 to S1 decreased ($p < 0.05$).

Figure 7(b) presents the changes in state transitions for S7. During the immediate-term interval, the transition probabilities from S7 to S1 and S4 significantly decreased ($p < 0.05$), while the transition probabilities from S7 to S2, S3, S5, and S9 increased ($p < 0.05$). The transition probabilities from S1 and S6 to S7 decreased ($p < 0.05$), while the transition probabilities from S5 and S9 to S7 increased ($p < 0.05$). During the short-term interval, the transition probabilities from S7 to S1, S3, and S9 decreased ($p < 0.05$). The transition probabilities from S1 and S9 to S7 decreased ($p < 0.05$), while the transition probability from S4 to S7 increased ($p < 0.05$).

Our results above showed that there is a dynamic reconfiguration pattern for transitions between brain states. The probability of transition between state 1 and state 7 weakened and continued until 80 minutes. The changes in state transitions decreased from immediately to 80 min after cTBS.

IV. Discussion

This study investigated the immediate and short-term changes in behavior and brain dynamics induced by cTBS. An HMM-based analytical framework was proposed to identify nine brain states from resting EEG data before stimulation (Pre), immediately after cTBS (I-Post), and 80 minutes after cTBS (S-Post). We found that cTBS not only induced behavioral changes that outlasted the stimulation period but also affected brain activities and organization of brain dynamics at different time points after cTBS. Additionally, cTBS altered temporal profiles of S1-S5 immediately after cTBS and temporal profiles of S5, S6 and S7 80 min after cTBS. Two specific states (presented here as S1 and S7) exhibited specificity in modulating completion times of the NHPT task for the left and right hands at different post-stimulation intervals. Furthermore, the transitions between S1 or S7 and other states showed dynamic reconfiguration during after-effects sustained time.

HMM-based brain states are believed to represent transient activations or deactivations of large-scale functional networks and have the advantage of assessing the spontaneous emergence of brain rhythms, i.e., large-scale oscillations of neuroelectric activity [34]. In this study, we investigated the neural dynamics mechanisms of these behavioral changes induced by cTBS through hidden Markov modeling of EEG power envelopes. Our study successfully identified nine HMM states, the majority of which exhibited relatively high average similarity across Pre, I-Post and S-Post sessions. These HMM states identified EEG power modulations within well-known

intrinsic functional networks, including the frontoparietal control network, bilateral auditory network, and visual occipital network. In addition, three HMM states (S2, S5, and S6) involving activation in the frontal and central regions showed slightly low average similarity across three sessions, which indicated that cTBS induced a change in spatial activation in the sensorimotor network and frontoparietal control network.

The global statistics derived from HMM state dynamics have a slightly different neurophysiologic significance [41]. For example, the frequency of occurrence of a particular state may reflect the tendency of its underlying neural generator to become activated. Hence, the reduction in the state occurrence and fractional occupancy and the increase in the state interval time can be considered disengagement and instability of the neural activity of the large-scale functional network. Conversely, an increase in state occurrence and fractional occupancy and a reduction in state interval time may be a sign of dysfunctional hyperactivity of the functional network. S1, S2, and S3 occurred less often with longer intervals immediately after cTBS. S4 and S5 occurred more often with short intervals immediately after cTBS, leading to a greater presence of S4 and S5. The increment in the percentage of total time of S4 and S5 was still maintained 80 min after cTBS, S6 and S7 occurred less often, and the interval time lasted longer. In other words, S1, S2, S3, S6 and S7 showed dysfunctional hyperactivity of the functional network, while S4 and S5 showed instability of the neural activity of the large-scale functional network. These findings suggested that cTBS can modulate the temporal stability of HMM states.

In this work, the observed alteration of HMM states provided correlation evidence with the behavioral performance caused by cTBS. In particular, the left-hand completion time of NHPT positively correlated with the occurrence of S1 and negatively correlated with the interval time of S1 immediately after cTBS. The HMM-based S1 was characterized as the activation of right occipito-temporal area. Also, S2 was also characterized as the activation of right occipito-temporal area. From the topographic map, the HMM-based S1 and S2 jointly represent the activation of microstate B as shown in our previous study [32]. Indeed, in previous study, we found that microstate B shows the greatest variation in the immediate effects of CTBS, and the average occurrence rate during immediate effects is positively correlated with left hand NHPT performance. Although state temporal characteristics of S1 and S2 changed significantly in the I-post in this work, only S1 is correlated with behavioral performance during immediate effects. Therefore, our findings in this study further emphasis that the right occipito-temporal area activation, especially S1, plays a key role in modulating motor performance during immediate effects after cTBS and that the HMM-based analysis method provides more refined detection of states on a temporal and spatial scale. Importantly, we also found some new results of short-term effect of cTBS. The average occurrence rate of the HMM-based S1 during immediate effects is positively correlated with left hand NHPT performance. The interval time of the HMM-based S1 during immediate effects is negatively correlated with left hand NHPT performance. These two correlations become weaker from I-post to S-post (Occurrence rate: I-post: $r=0.38$, $p=0.009$; S-post: $r=0.24$, $p=0.12$; Interval time: I-post: $r=-0.36$, $p=0.016$; S-post: $r=-0.26$, $p=0.07$). The changes in the dynamic characterization of state 1 are related to the impact of cTBS on left-handed behavior and these changes weaken with the weakening of aftereffect of cTBS. These results indicate that the dynamic characteristics of state 1 are potential biomarkers for characterizing the aftereffect changes of cTBS. Moreover, we also found that the average occurrence rate of the HMM-based state 7 during short-term effects is positively correlated with right-hand NHPT performance. This result was also not found in our previous research [32]. In addition, compared with results from previous study, the above research results indicate that the recognition of finer states in HMM helps us to gain a deeper understanding of the dynamic response of the brain to cTBS.

After cTBS over the left motor area, the left hand shows a decrease and then an increase in completion time, which may be due to the gradual weakening of the immediate effect following the stimulus over time. For the right hand, the completion time decreases with the increase in time, reflecting the adaptability and skill enhancement in repeated practice. Thus, the significant improvement in the right hand during the S-Post period may be due to repeated practice. Although cTBS induced significant changes of behavior performance, the behavioral differences before and after cTBS are relatively small. This may be attributed to the following two reasons: 1) Our study involved a healthy population. All participants were right-handed and we simulated the right motor area as functionally weaker area. Therefore, the enhancement effect for the left-hand is limited. 2) We assessed the effect of a single cTBS session. Compared to future continuous rehabilitation courses for stroke recovery, the effect of a single session is limited.

Previous studies have suggested that improvements in motor function after stroke rely on a balance of neuronal activity between the two cerebral hemispheres, which may be accomplished via reciprocal inhibition [39], [40]. In our study, we can hypothesize that after cTBS stimulation to the left motor cortex, there is a decrease in the proportion of activation in the left motor cortex, leading to reduced excitability, while there is an increase in the proportion of activation in the right motor cortex, leading to heightened excitability, thereby promoting improvement in left-hand NHPT performance. Our results showed that the activation regions of S2 (associated with activation in the left motor cortex) and S6 (associated with activation in the left sensorimotor area) may be located near the actual stimulation site, resulting in more pronounced spatial modulation effects and lower average similarity across the three sessions. Moreover, the results showed a lower presence of S2 and S6 after cTBS than before cTBS. Additionally, S4 (associated with activation in the right motor cortex) showed more presence during EEG recordings. These findings emphasized the inhibitory regulation of the contralateral hemisphere's brain activity in relation to the enhancement of motor abilities on the ipsilateral side. cTBS not only has local

but also remote effects, and these remote effects are probably mediated via interhemispheric inhibition.

Furthermore, we focused on the transition trajectory of S1 or S7 and analyzed the transition probabilities with other HMM microstates. We found significant changes in transition probabilities between the S1 and S7 states and most other states within the immediate term, which showed a reorganization of motor-related network states. As the after-effects persist of cTBS, there were fewer interactions with states showing significant transition probability changes associated with S1 and S7, which showed adaptive compensation during the process of restoring the brain's original equilibrium disrupted by cTBS. Combined with a previous study [45], our findings suggested that cTBS leads to increased selective integration within sensory-motor regions and reduced communication with other networks. Reconfiguration and rebalancing of brain microstates may be a possible neurophysiological basis of motor function improvement induced by cTBS.

V. Conclusion

In summary, we have provided evidence for altered brain dynamics after cTBS in healthy subjects over the left motor cortex. Our results reveal that cTBS modulates the spatial signature and temporal activities of HMM states. These findings suggest that the HMM approach can capture the intricate and diverse temporal dynamics of brain states modulated by cTBS, offering novel insights into understanding these biological and neural mechanisms. In future research, it is necessary to improve the Hidden Markov Model (HMM) method to enhance the robustness and reliability of the results. And, more participants and stroke patients should be recruited to validate the findings of this study. Moreover, the effects of continuous theta burst stimulation (cTBS) or repetitive transcranial magnetic stimulation (rTMS) beyond 80 minutes should also be further investigated. Finally, this work may provide a new tool for brain state monitoring based on electroencephalography (EEG), which can be used for detection and assessment in various research areas related to this field.

References

[1] A. T. Barker, R. Jalinous, and I. L. Freeston, "Non-invasive magnetic stimulation of human motor cortex," *Lancet*, vol. 325, no. 8437, pp. 1106–1107, May 1985.

[2] S. M. Brodie, S. Meehan, M. R. Borich, and L. A. Boyd, "5 Hz repetitive transcranial magnetic stimulation over the ipsilesional sensory cortex enhances motor learning after stroke," *Frontiers Hum. Neurosci.*, vol. 8, p. 143, Mar. 2014.

[3] R. Chen et al., "Depression of motor cortex excitability by low-frequency transcranial magnetic stimulation," *Neurology*, vol. 48, no. 5, pp. 1398–1403, May 1997.

[4] N. Sasaki, S. Mizutani, W. Kakuda, and M. Abo, "Comparison of the effects of high- and low-frequency repetitive transcranial magnetic stimulation on upper limb hemiparesis in the early phase of stroke," *J. Stroke Cerebrovascular Diseases*, vol. 22, no. 4, pp. 413–418, May 2013.

[5] J. Du et al., "Effects of high- and low-frequency repetitive transcranial magnetic stimulation on motor recovery in early stroke patients: Evidence from a randomized controlled trial with clinical, neurophysiological and functional imaging assessments," *NeuroImage, Clin.*, vol. 21, Jan. 2019, Art. no. 101620.

[6] S. W. Wu, "Effects of 30 Hz theta burst transcranial magnetic stimulation on the primary motor cortex," *J. Neurosci. Methods*, vol. 208, no. 2, pp. 161–164, 2012.

[7] Y.-Z. Huang, M. J. Edwards, E. Rounis, K. P. Bhatia, and J. C. Rothwell, "Theta burst stimulation of the human motor cortex," *Neuron*, vol. 45, no. 2, pp. 201–206, Jan. 2005.

[8] Y.-Z. Huang, R.-S. Chen, J. C. Rothwell, and H.-Y. Wen, "The after-effect of human theta burst stimulation is NMDA receptor dependent," *Clin. Neurophysiol.*, vol. 118, no. 5, pp. 1028–1032, May 2007.

[9] J.-P. Lefaucheur et al., "Evidence-based guidelines on the therapeutic use of repetitive transcranial magnetic stimulation (rTMS): An update (2014–2018)," *Clinical Neurophysiol.*, vol. 131, no. 2, pp. 474–528, 2020.

[10] L. Oberman, D. Edwards, M. Eldaief, and A. Pascual-Leone, "Safety of theta burst transcranial magnetic stimulation: A systematic review of the literature," *J. Clin. Neurophysiol.*, vol. 28, no. 1, pp. 67–74, Feb. 2011.

[11] V. Di Lazzaro et al., "Theta-burst repetitive transcranial magnetic stimulation suppresses specific excitatory circuits in the human motor cortex," *J. Physiol.*, vol. 565, no. 3, pp. 945–950, 2005.

[12] S. J. Ackerley, C. M. Stinear, P. A. Barber, and W. D. Byblow, "Combining theta burst stimulation with training after subcortical stroke," *Stroke*, vol. 41, no. 7, pp. 1568–1572, Jul. 2010.

[13] T. Nyffeler et al., "Theta burst stimulation in neglect after stroke: Functional outcome and response variability origins," *Brain*, vol. 142, no. 4, pp. 992–1008, Apr. 2019.

[14] S. Rizk et al., "Network mechanisms of responsiveness to continuous theta-burst stimulation," *Eur. J. Neurosci.*, vol. 38, no. 8, pp. 3230–3238, 2013.

[15] A. Pascual-Leone et al., "Characterizing brain cortical plasticity and network dynamics across the age-span in health and disease with TMS-EEG and TMS-fMRI," *Brain Topography*, vol. 24, nos. 3–4, pp. 302–315, Oct. 2011.

[16] T. V. Ilić and U. Ziemann, "Exploring motor cortical plasticity using transcranial magnetic stimulation in humans," *Ann. New York Acad. Sci.*, vol. 1048, no. 1, pp. 175–184, Jun. 2005.

[17] J. F. M. Müller-Dahlhaus, Y. Orekhov, Y. Liu, and U. Ziemann, "Interindividual variability and age-dependency of motor cortical plasticity induced by paired associative stimulation," *Exp. Brain Res.*, vol. 187, no. 3, pp. 467–475, May 2008.

[18] P. H. Ellaway, N. J. Davey, D. W. Maskill, S. R. Rawlinson, H. S. Lewis, and N. P. Anissimova, "Variability in the amplitude of skeletal muscle responses to magnetic stimulation of the motor cortex in man," *Electroencephalogr. Clin. Neurophysiol./Electromyography Motor Control*, vol. 109, no. 2, pp. 104–113, Apr. 1998.

[19] M. M. Shafi, M. B. Westover, M. D. Fox, and A. Pascual-Leone, "Exploration and modulation of brain network interactions with noninvasive brain stimulation in combination with neuroimaging," *Eur. J. Neurosci.*, vol. 35, no. 6, pp. 805–825, Mar. 2012.

[20] V. K. Kimiskidis, "Transcranial magnetic stimulation (TMS) coupled with electroencephalography (EEG): Biomarker of the future," *Revue Neurologique*, vol. 172, no. 2, pp. 123–126, Feb. 2016.

[21] N. C. Rogasch and P. B. Fitzgerald, "Assessing cortical network properties using TMS–EEG," *Hum. Brain Mapping*, vol. 34, no. 7, pp. 1652–1669, Jul. 2013.

[22] M. D. Greicius, B. Krasnow, A. L. Reiss, and V. Menon, "Functional connectivity in the resting brain: A network analysis of the default mode hypothesis," *Proc. Nat. Acad. Sci. USA*, vol. 100, no. 1, pp. 253–258, Jan. 2003.

[23] G. Deco, V. K. Jirsa, and A. R. McIntosh, "Emerging concepts for the dynamical organization of resting-state activity in the brain," *Nature Rev. Neurosci.*, vol. 12, no. 1, pp. 43–56, Jan. 2011.

[24] R. M. Birn, "The role of physiological noise in resting-state functional connectivity," *NeuroImage*, vol. 62, no. 2, pp. 864–870, Aug. 2012.

[25] F. Ferrarelli and M. L. Phillips, "Examining and modulating neural circuits in psychiatric disorders with transcranial magnetic stimulation and electroencephalography: Present practices and future developments," *Amer. J. Psychiatry*, vol. 178, no. 5, pp. 400–413, May 2021.

[26] Y. Zhong et al., "Simultaneously stimulating both brain hemispheres by rTMS in patients with unilateral brain lesions decreases interhemispheric asymmetry" *Restorative Neurol. Neurosci.*, vol. 39, pp. 409–418, Jan. 2021.

[27] Q. Ding et al., "Intermittent theta burst stimulation increases natural oscillatory frequency in ipsilesional motor cortex post-stroke: A transcranial magnetic stimulation and electroencephalography study," *Frontiers Aging Neurosci.*, vol. 14, Feb. 2022, Art. no. 818340.

[28] J. Jin, X. Wang, H. Wang, Y. Li, Z. Liu, and T. Yin, "Train duration and inter-train interval determine the direction and intensity of high-frequency rTMS after-effects," *Frontiers Neurosci.*, vol. 17, Jul. 2023, Art. no. 1157080.

[29] G. Thut and A. Pascual-Leone, "A review of combined TMS-EEG studies to characterize lasting effects of repetitive TMS and assess their usefulness in cognitive and clinical neuroscience," *Brain Topography*, vol. 22, no. 4, pp. 219–232, Jan. 2010.

[30] L. H. A. Strens, A. Oliviero, B. R. Bloem, W. Gerschlager, J. C. Rothwell, and P. Brown, "The effects of subthreshold 1 Hz repetitive TMS on cortico-cortical and interhemispheric coherence," *Clin. Neurophysiol.*, vol. 113, no. 8, pp. 1279–1285, Aug. 2002.

[31] S. Qiu, W. Yi, S. Wang, C. Zhang, and H. He, "The lasting effects of low-frequency repetitive transcranial magnetic stimulation on resting state EEG in healthy subjects," *IEEE Trans. Neural Syst. Rehabil. Eng.*, vol. 28, no. 4, pp. 832–841, Apr. 2020.

[32] S. Qiu et al., "Continuous theta-burst stimulation modulates resting-state EEG microstates in healthy subjects," *Cognit. Neurodynamics*, vol. 16, no. 3, pp. 621–631, Jun. 2022.

[33] B. Hunyadi, M. W. Woolrich, A. J. Quinn, D. Vidaurre, and M. De Vos, "A dynamic system of brain networks revealed by fast transient EEG fluctuations and their fMRI correlates," *NeuroImage*, vol. 185, pp. 72–82, Jan. 2019.

[34] N. Coquelet et al., "Microstates and power envelope hidden Markov modeling probe bursting brain activity at different timescales," *NeuroImage*, vol. 247, Feb. 2022, Art. no. 118850.

[35] D. Vidaurre, S. M. Smith, and M. W. Woolrich, "Brain network dynamics are hierarchically organized in time," *Proc. Nat. Acad. Sci. USA*, vol. 114, no. 48, pp. 12827–12832, Nov. 2017.

[36] A. J. Quinn, D. Vidaurre, R. Abeysuriya, R. Becker, A. C. Nobre, and M. W. Woolrich, "Task-evoked dynamic network analysis through hidden Markov modeling," *Frontiers Neurosci.*, vol. 12, p. 603, Aug. 2018.

[37] C. M. Michel and T. Koenig, "EEG microstates as a tool for studying the temporal dynamics of whole-brain neuronal networks: A review," *NeuroImage*, vol. 180, pp. 577–593, Oct. 2018.

[38] J. Liepert, S. Zittel, and C. Weiller, "Improvement of dexterity by single session low-frequency repetitive transcranial magnetic stimulation over the contralesional motor cortex in acute stroke: A double-blind placebo-controlled crossover trial," *Restorative Neurol. Neurosci.*, vol. 25, nos. 5–6, pp. 461–465, 2007.

[39] R. Sparing, M. Thimm, M. D. Hesse, J. Küst, H. Karbe, and G. R. Fink, "Bidirectional alterations of interhemispheric parietal balance by non-invasive cortical stimulation," *Brain*, vol. 132, no. 11, pp. 3011–3020, Nov. 2009.

[40] M. Corti, C. Patten, and W. Triggs, "Repetitive transcranial magnetic stimulation of motor cortex after stroke: A focused review," *Amer. J. Phys. Med. Rehabil.*, vol. 91, no. 3, pp. 254–270, Mar. 2012.

[41] D. Vidaurre, A. J. Quinn, A. P. Baker, D. Dupret, A. Tejero-Cantero, and M. W. Woolrich, "Spectrally resolved fast transient brain states in electrophysiological data," *NeuroImage*, vol. 126, pp. 81–95, Feb. 2016.

[42] Z. Liu et al., "Characteristics of EEG microstate sequences during propofol-induced alterations of brain consciousness states," *IEEE Trans. Neural Syst. Rehabil. Eng.*, vol. 30, pp. 1631–1641, 2022.

[43] T. Yan et al., "Effects of microstate dynamic brain network disruption in different stages of schizophrenia," *IEEE Trans. Neural Syst. Rehabil. Eng.*, vol. 31, pp. 2688–2697, 2023.

[44] F. Zappasodi et al., "Prognostic value of EEG microstates in acute stroke," *Brain Topography*, vol. 30, no. 5, pp. 698–710, Sep. 2017.

[45] G. Hartwigsen and L. J. Volz, "Probing rapid network reorganization of motor and language functions via neuromodulation and neuroimaging," *NeuroImage*, vol. 224, Jan. 2021, Art. no. 117449.

[46] A. P. Baker et al., "Fast transient networks in spontaneous human brain activity," *eLife*, vol. 3, Mar. 2014, Art. no. e01867.